AFRL-RQ-WP-TP-2013-0074

HORIZONTAL TWO PHASE FLOW REGIME IDENTIFICATION: COMPARISON OF PRESSURE SIGNATURE, ELECTRICAL CAPACITANCE TOMOGRAPHY (ECT) AND HIGH SPEED VISUALIZATION (POSTPRINT)

Paul J. Kreitzer

UES Inc.

Michael Hanchak

University of Dayton Research Institute

Larry W. Byrd

Mechanical and Thermal Systems Branch
Power and Control Division

NOVEMBER 2012

STINFO COPY

AIR FORCE RESEARCH LABORATORY
AEROSPACE SYSTEMS DIRECTORATE
WRIGHT-PATTERSON AIR FORCE BASE, OH 45433-7542
AIR FORCE MATERIEL COMMAND
UNITED STATES AIR FORCE

REPORT DOCUMENTATION PAGE

Form Approved
OMB No. 0704-0188

The public reporting burden for this collection of information is estimated to average 1 hour per response, including the time for reviewing instructions, searching existing data sources, searching existing data sources, gathering and maintaining the data needed, and completing and reviewing the collection of information. Send comments regarding this burden estimate or any other aspect of this collection of information, including suggestions for reducing this burden, to Department of Defense, Washington Headquarters Services, Directorate for Information Operations and Reports (0704-0188), 1215 Jefferson Davis Highway, Suite 1204, Arlington, VA 22202-4302. Respondents should be aware that notwithstanding any other provision of law, no person shall be subject to any penalty for failing to comply with a collection of information if it does not display a currently valid OMB control number. **PLEASE DO NOT RETURN YOUR FORM TO THE ABOVE ADDRESS.**

1. REPORT DATE *(DD-MM-YY)*	2. REPORT TYPE	3. DATES COVERED *(From - To)*
November 2012	Conference Paper Postprint	01 October 2011 – 30 April 2012

4. TITLE AND SUBTITLE
HORIZONTAL TWO PHASE FLOW REGIME IDENTIFICATION: COMPARISON OF PRESSURE SIGNATURE, ELECTRICAL CAPACITANCE TOMOGRAPHY (ECT) AND HIGH SPEED VISUALIZATION (POSTPRINT)

5a. CONTRACT NUMBER
In-house

5b. GRANT NUMBER

5c. PROGRAM ELEMENT NUMBER
62203F

6. AUTHOR(S)
Paul J. Kreitzer (UES Inc.)
Michael Hanchak (UDRI)
Larry W. Byrd (AFRL/RQQM)

5d. PROJECT NUMBER
3145

5e. TASK NUMBER
N/A

5f. WORK UNIT NUMBER
Q0LA

7. PERFORMING ORGANIZATION NAME(S) AND ADDRESS(ES)

UES Inc.
4401 Dayton-Xenia Road
Dayton, OH 45432

University of Dayton Research
Institute (UDRI)
300 College Park Avenue
Dayton, OH 45469

Mechanical and Thermal Systems Branch (AFRL/RQQM)
Power and Control Division
Air Force Research Laboratory, Aerospace Systems Directorate
Wright-Patterson Air Force Base, OH 45433-7542
Air Force Materiel Command, United States Air Force

8. PERFORMING ORGANIZATION REPORT NUMBER

AFRL-RQ-WP-TP-2013-0074

9. SPONSORING/MONITORING AGENCY NAME(S) AND ADDRESS(ES)

Air Force Research Laboratory
Aerospace Systems Directorate
Wright-Patterson Air Force Base, OH 45433-7542
Air Force Materiel Command
United States Air Force

10. SPONSORING/MONITORING AGENCY ACRONYM(S)
AFRL/RQQM

11. SPONSORING/MONITORING AGENCY REPORT NUMBER(S)
AFRL-RQ-WP-TP-2013-0074

12. DISTRIBUTION/AVAILABILITY STATEMENT
Approved for public release; distribution unlimited.

13. SUPPLEMENTARY NOTES
PA Case Number: 88ABW-2012-2864; Clearance Date: 18 May 2012. Conference paper published in the Proceedings of the ASME 2012 International Mechanical Engineering Congress & Exposition, conference held 9 - 15 November 2012 in Houston, Texas.

All references in this report to Air Force division AFRL/RZ refer to AFRL/RQ. This paper contains color.

© 2012 ASME. The U.S. Government is joint author of the work and has the right to use, modify, reproduce, release, perform, display, or disclose the work.

14. ABSTRACT
A two phase flow experimental test rig has been developed at the Air Force Research Laboratory, providing a closed loop refrigeration system capable of producing flow regimes from bubbly through annular flow. Two phase flow is produced by pumping subcooled R134a through a heat exchanger with 40 minichannels into an adiabatic transparent fused quartz observation channel with a hydraulic diameter of 7 mm. Refrigerant mass flux is varied from 100-400 kg/m^2s with a heat flux from 0-15.5 W/cm^2. Temperatures ranged from 18-25 °C and pressures between 550-750 kPa. The data from high speed pressure transducers were analyzed using standard signal processing techniques to identify the different flow regimes. Initial results indicate that different flow regimes can be identified from their pressure signature. In addition, real-time void fraction measurements were taken using Electrical Capacitance Tomography (ECT). This paper describes the process behind ECT systems used to measure two phase flow conditions. Comparisons with high speed video assess the accuracy of ECT measurements in identifying various two phase flow conditions. Results indicate variations between ECT and high speed images, however, enough information is provided to create flow pattern maps and regime identification for different superficial vapor and liquid velocities.

15. SUBJECT TERMS
two phase flow, flow regimes, heat transfer, flow boiling, electrical capacitance tomography, ECT

16. SECURITY CLASSIFICATION OF:

a. REPORT	b. ABSTRACT	c. THIS PAGE	17. LIMITATION OF ABSTRACT:	18. NUMBER OF PAGES
Unclassified	Unclassified	Unclassified	SAR	18

19a. NAME OF RESPONSIBLE PERSON (Monitor)
Travis E. Michalak

19b. TELEPHONE NUMBER *(Include Area Code)*
N/A

Standard Form 298 (Rev. 8-98)
Prescribed by ANSI Std. Z39-18

IMECE2012-89075

HORIZONTAL TWO PHASE FLOW REGIME IDENTIFICATION: COMPARISON OF PRESSURE SIGNATURE, ELECTRICAL CAPACITANCE TOMOGRAPHY (ECT) AND HIGH SPEED VISUALIZATION

Paul J. Kreitzer
Aerospace Power & Propulsion Technologies Division
UES Inc.
Dayton, Ohio 45432
Paul.kreitzer.ctr@wpafb.af.mil

Michael Hanchak
Modeling and Simulation Group
University of Dayton Research Institute
Dayton, Ohio 45469
Michael.hanchak.ctr@wpafb.af.mil

Larry Byrd
Propulsion Directorate, AFRL/RZPS
U.S. Air Force Research Laboratory
Wright Patterson Air Force Base, Ohio 45433
Larry.byrd@wpafb.af.mil

ABSTRACT

Understanding the behavior of transient two phase refrigerant flow is an important aspect of implementing vapor compression systems in future aerospace applications. Pressure drop and heat transfer coefficient are important parameters that guide the design process, and are influenced by flow regime. Published two phase flow models rely heavily on a priori knowledge of the current two phase flow conditions including flow regime. Additional complications arise when applying published correlations to a range of systems because each correlation is based on a specific set of experimental conditions, including working fluid, flow orientation, channel size, and channel shape. Non-intrusive measurement techniques provide important advantages while measuring the behavior of two phase flow systems.

A two phase flow experimental test rig has been developed at the Air Force Research Laboratory, providing a closed loop refrigeration system capable of producing flow regimes from bubbly through annular flow. Two phase flow is produced by pumping subcooled R134a through a heat exchanger with 40 minichannels into an adiabatic transparent fused quartz observation channel with a hydraulic diameter of 7 mm. Refrigerant mass flux is varied from 100-400 kg/m^{2}s with a heat flux from 0-15.5 W/cm^2. Temperatures ranged from 18-25 °C and pressures between 550-750 kPa. The data from high speed pressure transducers were analyzed using standard signal processing techniques to identify the different flow regimes. Initial results indicate that different flow regimes can be identified from their pressure signature. In addition, real-time void fraction measurements were taken using Electrical Capacitance Tomography (ECT). This paper describes the process behind ECT systems used to measure two phase flow conditions. Comparisons with high speed video assess the accuracy of ECT measurements in identifying various two phase flow conditions. Results indicate variations between ECT and high speed images, however, enough information is provided to create flow pattern maps and regime identification for different superficial vapor and liquid velocities.

NOMENCLATURE

α	=	Void fraction
A	=	Channel cross sectional area (m^2)
β_B	=	Empirical constant
D	=	Channel Diameter (m)
D_H	=	Hydraulic diameter (m)
d(j)	=	Detail coefficients
ε	=	Permittivity (F/m)
E_l	=	Energy density
Fs	=	Sample frequency

G	=	Total mass flux (kg/m^{2}s)
j	=	Volumetric flux based on flow area (m/s)
L	=	Channel length (m)
l	=	DWT level
n	=	Number of electrodes
N	=	Number of pressure data points
n_i	=	Empirical coefficient
p	=	Channel perimeter (m)
P	=	Pressure (kPa)
T	=	Temperature (C)
V	=	Voltage (V)
x	=	Quality
ρ	=	density (kg/m^3)

Subscripts

f	=	fluid
v	=	vapor

Acronyms

ECT	=	Electrical capacitance tomography
DWT	=	Discrete wavelet transform
fps	=	Frames per second
ID	=	Inner diameter
LBP	=	Linear back projection
OC	=	Observation channel

INTRODUCTION

Understanding two phase flow transitions and interactions is important in the development of advanced cooling systems. Applications include cooling techniques for computers, home/automotive air conditioning systems, avionics, industrial transport, and nuclear reactors[1-3]. Various flow and heating conditions will result in a wide array of flow behavior that can be classified into discrete flow regimes. Current models rely on a priori knowledge of the flow regime in order to apply proper correlations.

During laboratory testing optical access is not an issue; however, in final applications this might be difficult or impossible. Therefore, non-intrusive measurement techniques must be used to indicate the flow regime. Once a flow regime identification method is developed it can be used to classify pressure drop and heat transfer correlations.

Tran et al.[4] tested two phase flow pressure drop for R-134a, R-12, and R-113 with channel inlet pressures ranging from 138 to 856 kPa. They tested two different channel geometries, with hydraulic diameters of 2.46 mm and 2.4 mm with round and rectangular cross sections respectively. A pressure drop correlation was developed based on experimental data to an error of ± 20%. However, comparison with state-of-the-art correlations failed to accurately predict the experimental data; showing wide variation between correlations produced by similar experimental techniques.

Lee and Garimella[5] tested flow boiling in microchannel arrays with a hydraulic diameter of 0.6 mm using deionized water. Comparisons between experimental data and published correlations provided mean absolute error (MAE) from 16.4% to 55.1%. Based on these correlations a new correlation was developed to have an MAE of 11.4%. These correlations were based on the assumption of micro/mini channels with laminar-laminar flow conditions. Therefore, these correlations are not expected to translate well to larger channel sizes; demonstrating the need for a general method for comparing experimental data.

Brutin et al.[6] investigated the unsteady behavior of pressure signals in single microchannel flow of n-pentane. Their research revealed pressure fluctuations from 20 to 100 kPa/m with frequencies ranging from 3.6 to 6.6 Hz. However, this study focused on detecting flow reversal due to unsteady boiling behavior experiencing slug flow. This technique might be useful for differentiating flow regimes.

Quiben and Thome[7] developed an analytical model for horizontal two phase flow with evaporation. Their model is reliant on knowing the flow regime present in the channel in order to calculate the associated two phase pressure drop. The model is broken into eight separate flow regimes, requiring a priori knowledge of the flow regime in order to proceed. Unclear flow regime definitions leave room for subjective interpretation by researchers, demonstrating the need for a generalized method that can be used to differentiate between flow regimes.

Two phase flow behavior varies depending on the size and orientation of the channel. For this paper all flow is in the horizontal orientation. Characterization of the channel size is accomplished using the hydraulic diameter, D_H ($D_H=4A/p$), enabling a comparison between different shape channels. Channel classifications are broken down by size and include: macrochannels – D_H larger than 3 mm, minichannels – D_H less than 3 mm but larger than 1 mm, and microchannels – D_H less than 1 mm. Additional classifications and transition regions are described in the literature[1, 8].

There are two different methods of flow regime identification, direct and indirect[9]. Direct identification is a subjective method and is usually accomplished with visual techniques. Indirect identification uses analysis of measured signals to determine the flow regime. The current work will compare the results from a direct method, using a high speed video camera, with two indirect methods, Electrical Capacitance Tomography (ECT) analysis and pressure transducer signal analysis.

ECT is a non-invasive flow measurement technique and has been improving since its conception by the Department of Energy in the 1970s in Morgantown, WV[10]. However, commercial development did not take off until the late 1980s[11, 12]. ECT is a technique that consists of three main components: an externally mounted sensor containing n electrodes, the sensing and control electronics, and the computer interface used for controlling and interpreting the measurements.

Applications for ECT include two phase and three phase flow systems, including: fluidized beds, oil transport, mixing, and multiphase flow systems. Most of the research efforts at this point have been focused on industrial applications where qualitative results are sufficient. However, with improvements in computer capabilities, iterative methods can now be used to solve for permittivity distributions.

Pressure signal analysis is another method used for regime identification. Fourier analysis is a powerful tool for signal analysis and effectively transforms a time-based data signal into

the frequency domain by projecting the signal onto trigonometric basis functions of varying frequencies. Unfortunately, for non-stationary signals, that is, signals which change character when shifted in time, Fourier analysis alone is deficient since it confounds unequally-spaced time events into spurious frequency content.

Conversely, wavelet analysis provides tools to analyze signals in both time and frequency domains, by using the best traits of Fourier analysis without losing important time-based information. Instead of trigonometric basis functions, this type of analysis uses specific wavelet shape functions as bases. Not any shape is admissible as a wavelet function and strict adherence to design rules is required.

In the Discrete Wavelet Transform (DWT) a wavelet shape function is transformed by low-pass and high-pass filters. This provides two outputs: low-frequency "approximation" coefficients and high-frequency "detail" coefficients. Then, the coefficient vectors are down-sampled by a factor of two. This is the first level decomposition. This process is repeated by sending the new approximation coefficients through the same filters and again down-sampling to provide the second level decomposition. Thus, this scheme only provides scales based on powers of two. The magnitude of these coefficients represents how well the wavelet approximates the signal at specific times and frequency scales.

Wavelet transformations have been applied to fluid flow, in particular turbulence[13]. The two-phase, vertical flow of water and air was studied by Elperin and Klochko[14]. In that work, they laid out a methodology for future two-phase flow regime identification using the output of a DWT. Their analysis forms the basis of what is presented here. Tan[15] also studied vertical air/water flow; however, instead of pressure signals they recorded electrical resistance tomography data and then applied wavelet transformations. Furthermore, they used machine learning algorithms to identify the flow regime with ~90% accuracy. The mathematical details of wavelet analysis can be found in other works[13, 16-19].

The aim of this paper is to present two phase flow behavior of R134a in a horizontal channel, by documenting and comparing different analysis techniques for flow regime identification and pressure drop analysis. Results will be presented for both flow regime identification and pressure drop analysis.

EXPERIMENTAL FACILITY

The experimental test facility used for this research effort is a closed loop refrigeration system with two separate flow loops. Figure 1 presents the design schematic showing components used to create and maintain two phase flow, including: receiver, filter, positive displacement gear pump, micro-turbine flow meter, heat exchanger (with 40 minichannels $D_H = 1.4$ mm), observation channel ($D_H = 7$ mm), back pressure valve, and condenser. The system is also equipped with a bypass and over pressure containment tank. System temperatures and pressures are set for standard room temperature conditions with ample insulation in order to create adiabatic test conditions. A liquid-liquid heat exchanger connected to a constant temperature chiller is used to remove heat from the system.

Flow created from heating liquid refrigerant can be classified into one of seven flow regime categories. Baseline flow corresponds to pure liquid refrigerant flow. Bubbly flow is mostly liquid flow with small vapor bubbles. As the vapor bubbles grow and coalesce into bullet shaped vapor pockets they form plug flow. Slug flow occurs when the vapor pockets expand and occupy most of the channel diameter and are separated by fully filled liquid regions. Intermittent flow occurs when a full liquid fill no longer separates vapor pockets and large waves dominate. As the flow becomes smoother it transitions into stratified wavy flow. Finally as the flow begins to climb up the side walls of the channel annular wavy flow occurs. A more in depth description of the components and capabilities of the system was published previously by Kreitzer[20].
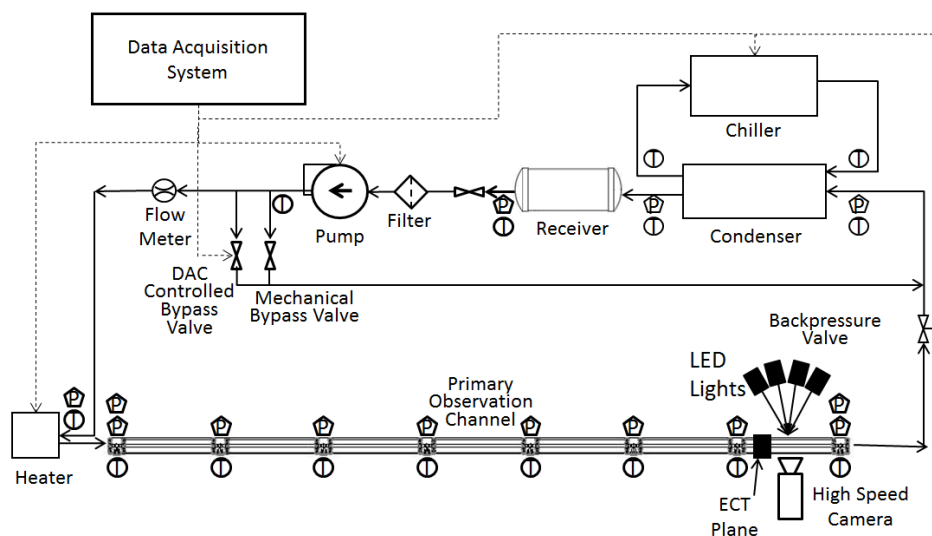
Figure 1. Experimental flow loop schematic, showing each of the flow components the dashed lines represent control singles from the DAC to the components.

The test rig is outfitted with various measurement devices including temperature and pressure measurement as indicated in Figure 1. Advanced measurement techniques include high speed video capabilities with automated image analysis software capable of tracking individual objects throughout the flow. Another technique that is being used to determine flow distribution and flow regimes is ECT. Both of these advanced measurement techniques will be discussed further in the next section. System performance is outlined in Table 1, showing the flow rates and heater powers that are attainable using this facility.

A. Uncertainty

The experimental test rig is outfitted with numerous thermocouples, pressure transducers and a flow meter. Omega Type T thermocouples were used and calibrated to ±0.1 °C using a Fluke constant temperature bath and Hart Scientific RTD over a range from 5 to 100 °C. Omega PX409 pressure transducers were calibrated to ±0.1% full scale using a Heise handheld pressure calibrator between 35 and 760 kPa. A McMillan micro-turbine flow meter was calibrated to 0.6 % full scale using Air Force standard F242007.

Table 1. System Capabilities.

Parameter	Test Range
Refrigerant	R-134a
Pump mass flux	$0 - 300$ kg/m^{2}s
Heater power	$0 - 1000$ W
Coolant delta T	$0 - 10$ °C
Saturation Temperature	$18 - 23$ °C
Saturation Pressure	$550 - 650$ kPa

MEASUREMENT TECHNIQUES

Determining the flow regime enables application of published frictional pressure drop and heat transfer coefficient correlations. Direct identification methods like high speed video analysis are the most common methods for verifying the flow regime present in a two phase flow system. However, in a real life application, directly viewing the flow path might be unsafe or even impossible. Therefore, indirect measurement techniques are needed to evaluate the current flow regime within a channel. Both ECT and pressure transducer wavelet analysis provide a non-intrusive technique that provide flow phase distribution and a method for identifying the proper flow regime.
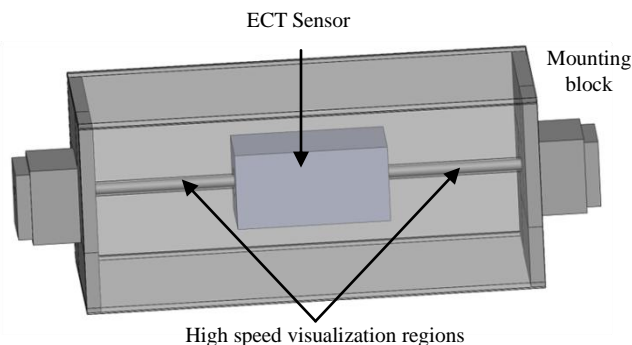
A. High Speed Video

Comparisons of ECT data with high speed video are imperative for determining the quality and accuracy of the measurements. A transparent quartz observation channel provides access for both measurement devices (Figure 2). Under a given flow condition a high speed video camera captures the behavior of two phase flow inside the channel. Different camera orientations have been used to provide imaging of the flow either entering or exiting the ECT sensor.

Close up imaging provides a high resolution that can be used to resolve fine details and track specific objects through the flow.

A Vision Research V4.2 high speed camera with an image resolution of 512 x 512 pixels was used for all visualizations. This camera uses a framing rate of 2,100 fps for full resolution and up to 90,000 fps with a reduced resolution. High intensity VIC LED lighting is used to backlight the channel to optimize image contrast and available depth of field.

Figure 2 presents a 0.305m section of the observation channel with measurement regions clearly marked. The location of the ECT sensor can be moved to accommodate different measurement techniques. Fused quartz glass tubing, ideal for visualization, as well as insulation for the ECT sensor, was selected as the observation channel material. Between each observation section is a mounting block provides access for pressure transducer and thermocouple measurements. The inner diameter of the mounting block was machined to the ID of the glass sections to provide a smooth transition from block to channel.


Figure 2. Single observation channel showing ECT sensor and high speed visualization regions.

Image analysis and tracking software provides an assessment of the various flow conditions achieved during testing. Image analysis techniques include object tracking where a specific point of interest in the flow, i.e. a bubble or vapor pocket, is tracked from frame to frame. Tracking can be performed semi-automatically; with proper scaling and calibration, position, velocity, and acceleration data can be determined. However, this technique remains subjective due to the lack of a standard volume size to be analyzed.

B. Electrical Capacitance Tomography

ECT sensors can have eight, 12, or 16 radially fixed electrodes around an insulating vessel. For simplicity and relevance to current research efforts, all measurements are described for an eight electrode round sensor with two phases within the measurement volume. Figure 3 shows the current configuration of the eight electrode sensor, insulating tube, ground screen and an enclosed measurement volume. The eight electrodes function as sender and receiver electrodes. Void fraction measurements are accomplished by sending a voltage into the measurement volume by the active sender electrode

and measuring the resultant electrical field through the receiver electrodes.
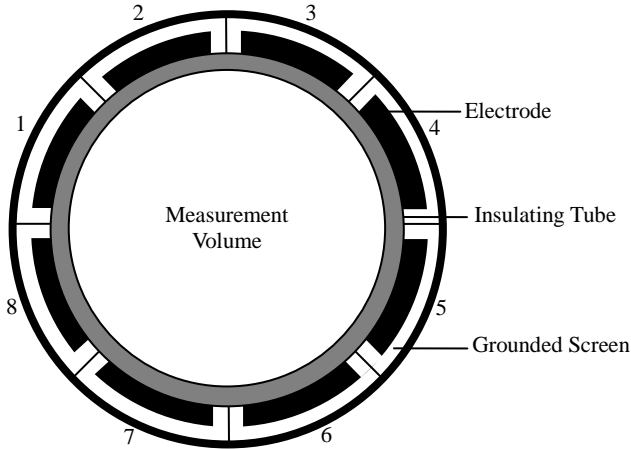
Figure 3. ECT Sensor with eight electrodes.

ECT measurements are able to discriminate between different phases within the measurement volume; given the two phases have different permittivity values. Liquid-vapor distributions of the two phase flow create unique electric fields inside the sensor, thus influencing the measured capacitance by each electrode in the sensor. Starting with electrode number one as the sender, a voltage signal is applied and the capacitance is measured from the remaining electrodes, 2-8. Next, electrode two becomes the sender and electrodes 3-8 become the receivers. This process is repeated around the sensor until all measurement pairs have been established, producing a diagonal measurement matrix. The number of measurements can be represented by the following equation [21]:

$$\frac{n(n-1)}{2} = \frac{8(8-1)}{2} = 28. \qquad (1)$$

Signal excitation results in voltage measurements between pairs of electrodes, indicating inherent capacitances [22]. Baseline reference values were taken while the sensor was liquid filled, indicating high permittivity ($\varepsilon=1$) and vapor filled, indicating low permittivity ($\varepsilon=0$). Permittivity measurements are then normalized between zero and one corresponding to the reference values. A non-linear electric field response may generate values outside this normalized range and must be coerced back to values of zero or one, based on reference conditions. It is then possible to convert the measurements into a color coded map of the measurement volume for visual observations (tomogram).

Sensitivity maps are created for each location within the measurement volume[11]. Sensitivity is defined as the propensity for capacitance of a given location to differ with the change of permittivity within the measurement volume. These maps represent the sensitivity of a particular location to detect a change in permittivity. The configurations and non-intrusive behavior of the sensor, results in greater sensitivity along the edges, closer to the electrodes, with less sensitivity near the center. As a result sharp contour changes between different phases are difficult to detect[11]. Reconstruction algorithms use these maps to linearize the measured capacitance values.

Two electrode grounding techniques are used with ECT measurements. The first technique grounds all of the receiving electrodes for a faster measurement cycle. The second grounding technique allows all the receiver electrodes to float relative to the electric field present; only grounding the electrode that is read. The second measurement technique is slower but produces more sensitive capacitance readings. Figure 4 presents an unwrapped sensor showing the electrodes. Wiring from the capacitance measurement box and individual electrode grounding is shown for electrode 1.
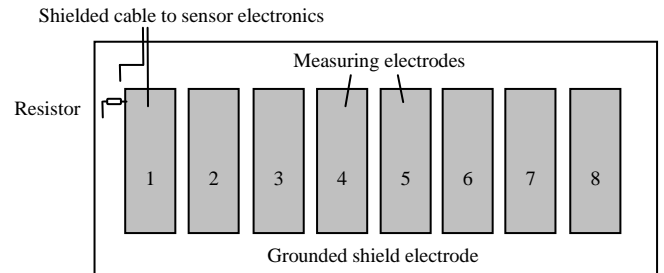
Figure 4. ECT electrode layout showing grounding and wiring for electrode 1.

Selection of the number of electrodes and the size of the electrodes is an important portion of the ECT process. The tomogram is a 2-D representation of a 3-D volume, as a result of the shape and size of the electrodes within the sensor. Depending on the size of the measurement volume, excess electrodes will reduce capacitance sensitivity between neighboring electrodes. Similarly, the length of the electrodes has a comparable effect. If the electrodes are too short an increased uncertainty in the capacitance measurements will result. If the electrodes are too long the reconstructed resolution will be diminished.

Two categories of algorithms are available for the reconstruction process: non-iterative and iterative[11, 12, 22-25]. The non-iterative algorithms include: linear back projection (LBP), singular value decomposition, and Tikhonov. These algorithms are fast and can be performed real-time but do not provide highly accurate reconstructions. The more involved iterative algorithms include: an algebraic reconstruction technique, Newton-Rapshson iterative Tikhonov, and Landweber iteration. These algorithms are slower and must be performed during post processing; they provide a more accurate reconstruction of the measurement volume. Results presented in this paper were analyzed using the LBP method.

A tomogram display is a 32 x 32 element area; for a square sensor this would produce 1024 elements while a round sensor only has 812 elements. Each element has three states. The first is for a measured value of one corresponding to a high ε phase. Second, is when the measured value is zero or low ε phase. Third is for transition and the value is between zero and one. Depending on the permittivity value, the resulting display color is changed; indicating the refrigerant state.

A useful benefit of ECT is the ability to combine a series of 2-D tomograms to create a pseudo 3-D representation of the flow. Stacked images allow a realistic visualization of the flow by stacking subsequent tomograms together. Comparing ECT results with those obtained from high speed video analysis is easily accomplished using this technique.

C. Pressure Transducer Signal Wavelet transformation

This section describes the application of the discrete wavelet transform to the pressure signal data. This type of analysis is especially useful when the data signal is non-stationary, that is, not regularly periodic. The method extracts both frequency and time information by comparing the signal to a predetermined wavelet function that is both scaled in length and shifted in time. These numerous comparisons result in coefficients that are further manipulated to provide characteristic values, which aid in signal identification.

Before applying any transformation, the original signal was conditioned using a low-pass filter. Fourier analysis revealed two spikes of energy at approximately 50 and 90 Hz that occur in all of the pressure signals. It was concluded that these were both due to unidentified mechanical component noise. Using the Matlab signal processing toolbox[26], a low-pass filter was designed for a cutoff frequency of 50 Hz. The filter, an FIR-type, was implemented using a zero-phase algorithm. An example of the filtering is shown in Figure 5.
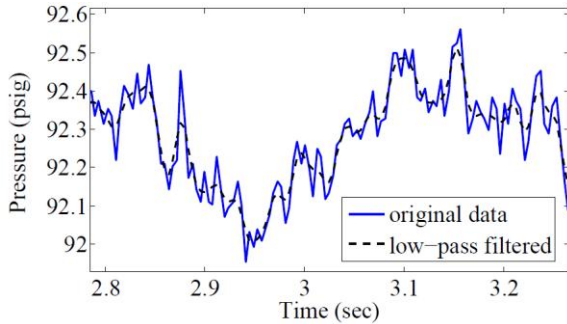
**Figure 5.** A representative image of the filtering applied to the raw pressure signal data.

In some cases, a noticeable linear trend was present in the raw data and can be attributed to an increasing environmental temperature. Even though this trend was less than 1°C/min, it moved additional relative energy to low frequencies. The linear least squares method was used to calculate the linear trend which was subsequently subtracted from the signal data, setting the mean of the signal to zero. While the mean pressure value is important for regime identification and determining saturation properties, it is not required for a frequency analysis. Finally, each signal was scaled by its standard deviation; allowing the following analysis to be plotted with the same axis limits.

In the DWT the signal is iteratively convolved with the wavelet filters and down-sampled, using the following steps:

1) Generate the wavelet scaling filter from the desired wavelet.

2) Generate the complimentary, orthogonal low-pass and high-pass filters.

3) Convolve both filters with the signal. The low-pass filter produces the approximation coefficients while the high-pass filter produces the details coefficients.

4) Down-sample the new approximation signal.

5) Repeat steps 3 and 4.

The MATLAB wavelet toolbox was used to generate appropriate wavelet scaling[26]. Following the work of Elperin[14], the Daubechies' wavelet of order four (*db4*) was chosen for its ability to represent the variety of flow regimes present in the experimental data. For more information on this family of wavelets, see Daubechies[16]. From the wavelet scaling function, low-pass and high-pass decomposition filters were generated using quadrature mirror filter decomposition. Figure 6 shows the wavelet shape and scaling functions as well as the resulting high and low pass filter vectors.
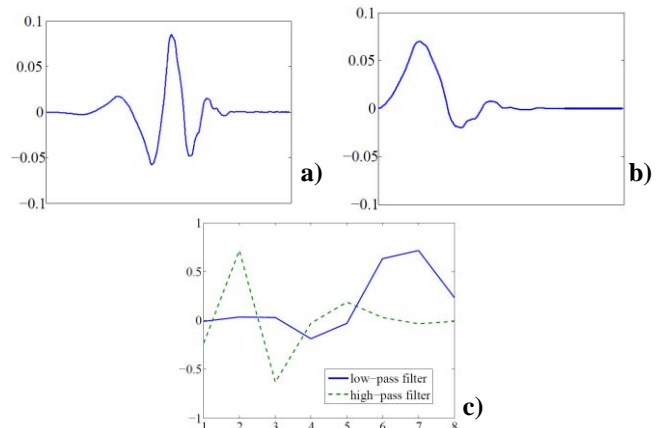
Figure 6. The *db4* wavelet shape function (a), scaling function (b), and high and low pass filter vectors (c).

The low frequency approximation coefficients are the convolution of the low-pass filter and the signal. The high frequency detail coefficients are the convolution of the high-pass filter and the signal. The discrete convolution of a signal *u* and a filter *v* is given by

$$w(k) = \sum_j u(j)v(k - j + 1) \qquad (2)$$

where both inputs have been zero-padded. The DWT retains only the central part of the convolution that is the same size as the original signal.

The approximation coefficients were down-sampled by removing every other data point. This effectively doubled the scale of the wavelet for the next iteration thereby revealing features at half the previous frequency. Continuing in this fashion produced approximations of the original signal with successively halved frequency content. For example, if the sample frequency is given by Fs, the first DWT produced an approximate signal with frequency content of Fs/2 and lower. The next DWT produced an approximation with frequencies less than Fs/4, etc.

This process cannot continue indefinitely as the successive down-sampling will eventually reduce the number of data points to one. Thus, the maximum number of DWTs to perform is given by floor(log2(N)), with N being the original number of data points; however, it was chosen to stop the process when the number of data points falls below a certain value. For the experimental data, eleven levels of deconstruction were used. Similar to Fourier transformation, the original signal can be perfectly reconstructed by reversing the process, namely, by up-sampling the last approximation and detail coefficient vectors, re-filtering each with the proper reconstruction filter, summing the results, and repeating[26].

At each DWT level, one is left with two vectors of coefficients. Define the energy density of a DWT by the sum of squares of the detail coefficients divided by the number of samples, i.e.,

$$E_l = \frac{1}{N}\sum_j d_l(j)^2, \quad l = 1,2,\dots,n_{levels} \quad (3)$$

Where l is a particular level of the DWT and the $d(j)$ are the detail coefficients at that level. By plotting these energies at each level, a characteristic map emerged that communicates the relative amount of energy within discrete frequency bands. This method of analysis is due to Elperin[14].

RESULTS

Three different measurement and analysis techniques were used to examine the two phase flow data presented in this paper. Figure 7 shows pressure data for each of the experimental flow regimes. This data was recorded directly before and after the ECT sensor to monitor the condition of the two phase flow. An L/D ratio of 285 was used for all ECT measurements. From this chart each flow regime has a different repeatable pressure signature. From the literature search a two phase flow of a compressed liquid and non-condensable gas should be fully developed before it reaches the measurement section[2, 27, 28]. The present system consists of a saturated liquid resulting in some phase change along the tube due to pressure drop but typically the flow structure is not changing by the end of the observation channel.

Figure 7 clearly shows that the frequency and amplitude of the pressure signal increases with changing flow regime. Bubbly flow shows an almost flat trend with little to no change of signal. As the heat flux is increased the flow regime transitions from bubbly to plug, slug, intermittent, stratified wavy, and annular. Plug flow starts to show periodic depressions during flow. During slug flow the amplitude of the deflections begins to increase and the frequency resembles the observed flow pattern. Stratified wavy flow produces larger peaks that are more spread out corresponding to the actual flow conditions where the flow is mostly separated in a turbulent manner with mostly small waves and an occasional large wave that fills the channel. Finally, looking at annular flow, the flow is fully separated with an increase in the size of the surface waves at the interface. Liquid refrigerant is seen flowing along the walls and top of the channel during this flow regime.
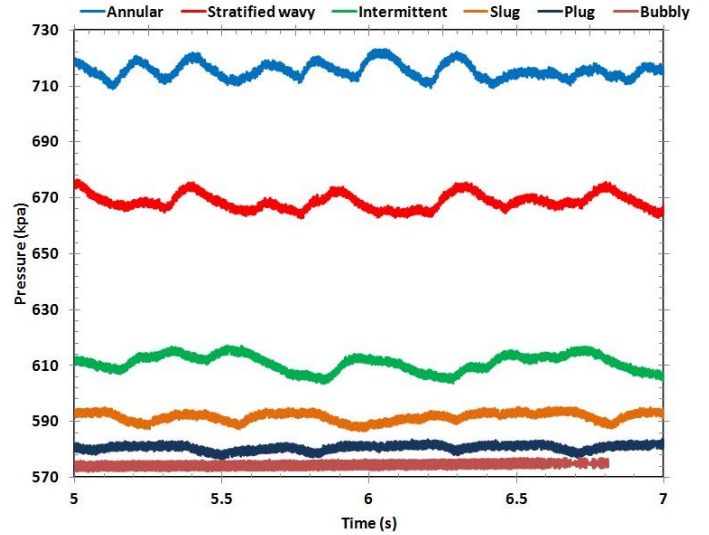

Figure 7. Pressure transducer data showing flow regime pressure signatures.

A. ECT Analysis Results

Simultaneous measurements using the high speed video camera and the ECT system were taken for each of the expected flow regimes. Two assumptions are used; fully developed flow in the final section of the observation channel, and the ECT sensor and the high speed video observes the same flow (see Figure 2). Therefore, direct comparisons between the high speed video images and the resulting tomograms or stacked tomograms should be reasonable.

Figure 8 shows a comparison between the ECT data in the form of a stacked tomogram with the high speed video. A stacked tomogram is a series of tomograms plotted as a function of time to provide a pseudo 3-D view of the flow traveling through the channel in the location of the sensor. In Figure 8 the flow is traveling from left to right. From this comparison the ECT does a good job representing the flow traveling through the channel within the sensor. Transition regions are slightly exaggerated in the ECT portion of Figure 8 because the electrodes within the sensor are about two inches in length and therefore represent a volume average of the flow. This averaging also explains why the small bubbles are not visible in the stacked tomogram.
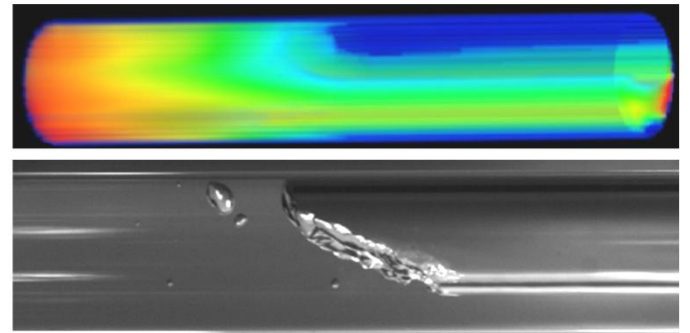
Figure 8. Stacked ECT tomogram (top) compared with a high speed video image (bottom) of the same flow.
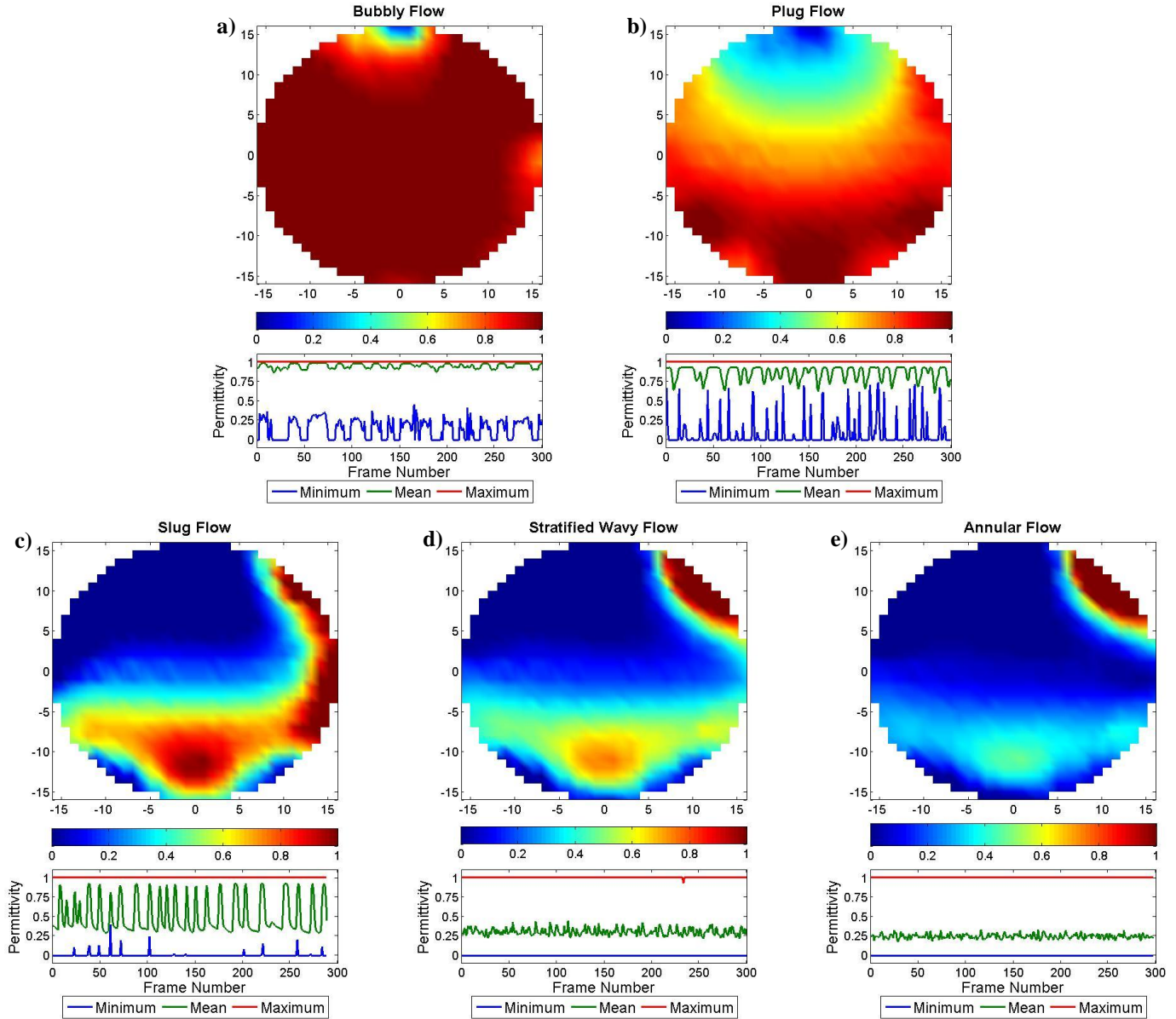
Figure 9. ECT Tomograms and permittivity distribution for a) bubbly, b) plug, c) slug, d) stratified wavy, and e) annular flow distributions.

Figure 9 presents results of ECT sampling during testing. The top portion of each section presents a tomogram, where dark blue corresponds to pure vapor and dark red corresponds to pure liquid; oranges, yellows, and greens represent transition regions. The bottom portion of each section presents the permittivity distribution during each flow regime and is displayed over time, indicated by frame number (sampled at 17.8 Hz). The red line indicates the maximum permittivity detected in the channel, while the blue line represents the minimum permittivity. Locations where the red line equals one indicate pure liquid present in the channel; similarly when the blue line equals zero pure vapor is present. The green line represents the mean permittivity of the entire tomogram for

each frame and the fluctuations indicate changing flow conditions.

Figure 9 a) corresponds to bubbly flow and shows a mostly liquid channel section with a small vapor pocket along the top. The permittivity plot shows that the vapor region tends to fluctuate indicating the passage of bubbles, while the mean permittivity remains relatively constant. As the flow transitions to plug flow, Figure 9 b), the vapor region at the top of the tomogram increases to reflect the larger size of the vapor pockets. The permittivity plot shows a more periodic behavior and fluctuations in the mean permittivity are reflected. Figure 9 c) presents slug flow with vapor present along the top of the tomogram and transition flow to mostly liquid along the bottom. An oversaturation region exists on the right hand top portion of

the tomogram. This region is present because of a minor manufacturing defect and always shows liquid present. The permittivity plot shows exaggerated semi-repeatable fluctuations for the mean permittivity, indicating a highly oscillating flow condition with the passage of vapor pockets separated by regions of full liquid slugs. Stratified wavy flow presented in Figure 9 d) shows vapor along the top of the channel with transition and a thinner liquid layer along the bottom. The permittivity plot for stratified wavy flow indicates that both vapor and liquid are always present in the channel. Examining the mean permittivity shows that the mean permittivity is approximately 30 percent. The fluctuations seen in the slug case have subsided and a smoother line is present. Finally, Figure 9 e) presents annular flow with similar conditions to the stratified wavy case, however with a thinner layer of liquid along the bottom of the tomogram. The mean permittivity value is smoothed out even more and indicates less oscillation in the flow.

Using the permittivity distribution data presented in Figure 7, a void fraction can be estimated from the ECT data assuming that the void fraction is one minus the mean permittivity. Table 2 shows a direct comparison between the ECT permittivity data, energy balance calculations for void fraction and high speed video analysis. The values from the ECT match very well the values calculated performing an energy balance. The data obtained from the high speed video is very subjective (visual estimate) and therefore is roughly the same as the ECT in each case.

**Table 2.** Void fraction comparison between analysis methods.

	ECT	Energy Balance	High Speed Video
Bubbly	6.3	4.3	5
Plug	13.1	15.4	10
Slug	46.6	43.2	40
St. Wavy	68.6	70.3	60
Annular	81.8	87.7	80

The calculations used for the void fraction using the energy balance were based on the Zivi model of the Butterworth form[29]. Where the empirical coefficients are defined as: $\beta_B = 1$, $n_1 = 1$, $n_2 = 0.67$, and $n_3 = 0$.

$$\alpha = \left[1 + \beta_B \left(\frac{1-x}{x} \right)^{n_1} \left(\frac{\rho_v}{\rho_l} \right)^{n_2} \left(\frac{\mu_l}{\mu_v} \right)^{n_3} \right]^{-1} \qquad (4)$$

B. Wavelet Analysis Results

Figure 10 shows relative energy densities per level for each of the seven flow regimes. A few observations can be made. First, the baseline case has most of its energy in the higher frequencies (lower DWT level). It is important to note that each plot is scaled to its own standard deviation and that the baseline case does not necessarily have more energy than the plug case. The shape of the distributions is the important distinction. Unfortunately, the baseline and bubbly cases appear indistinguishable. However, using the mean pressure signal, one could identify the difference in heater power between the two cases to identify the regime (Figure 7).
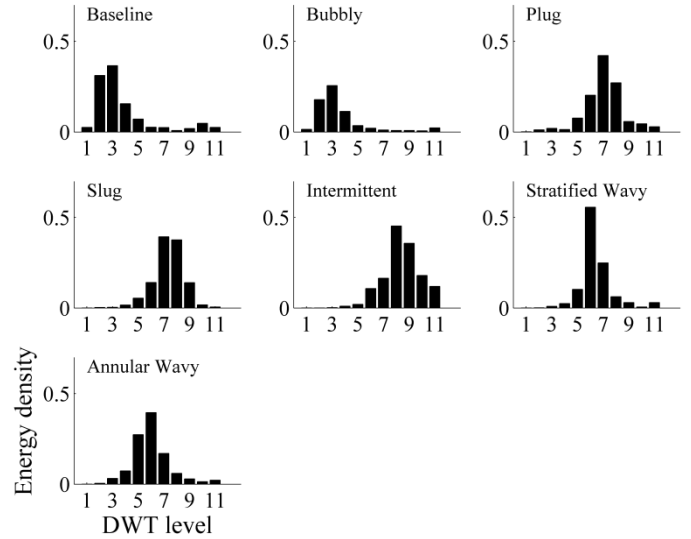
Figure 10. The result of DWT processing of the scaled data signals.

The plug flow regime is characterized by a Gaussian-like peak at level seven. Slug flow looks very similar to plug flow except there is almost equal energy at levels seven and eight. Intermittent flow has its peak energy at level eight with a wide distribution. The most peaked distributions occur in the stratified wavy flow regime with peaks at level six. The annular wavy flow also has a peak location at level six but with increasing wider distribution as the heat power increases.

Granted, these categories and distribution shapes are semi-qualitative at this point and depend on both the sample frequency and number of samples. Future work will be to implement an algorithm, such as in Tan[15], to automatically classify new data into the proper regime. Any scheme should also include the mean and standard deviations of the pressure signals.

C. Pressure Drop Results

Pressure drop was measured across the entire length of the channel described in the experimental setup previously. The pressure drop was seen to fluctuate based on the flow regime present, Figure 7, and therefore the pressure signal at each location had to be averaged before a pressure drop was calculated.

Figure 11 shows the measured pressure drop compared with five other common two phase pressure drop correlations available in the literature. This plot shows that most of the current correlations over predict the observed pressure drop; however, there is one that under predicts the pressure drop. Each of these correlations is based on an experiment with slightly different testing conditions. Comparing results of the current experimental data with the published results of Mishima and Hibiki[30] and Yu et al.[31] resulted in mean absolute (MAE) errors of 35% and 80% respectively. Comparing the results of Lee and Lee[32] vs Yu et al.[31] results in a MAE of 95%. The lack of consistency among the different correlations and with the

current data shows the need for a generalized pressure drop correlation that can be used across various geometries, sizes, shapes, and fluids. The use of steady state testing and flow regime identification could be used to improve the accuracy of pressure drop correlations and provide a more general application.
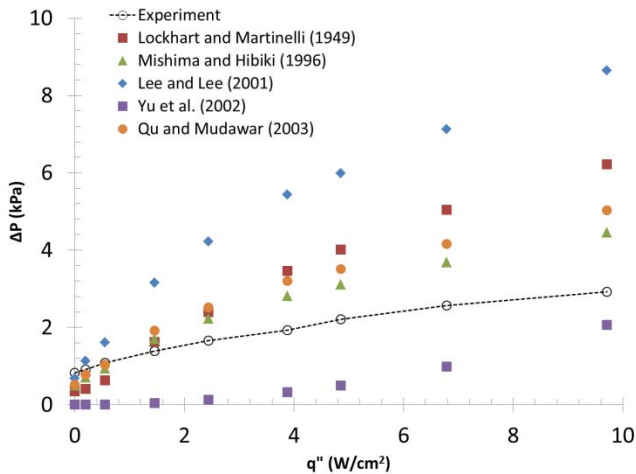

Figure 11. Pressure drop comparison with published correlations[30-34].

CONCLUSION

Three different techniques were used to identify the flow regime present in horizontal two phase flow, using both direct and indirect techniques. High speed visualizations were used as a baseline standard for comparison.

ECT proved to be the most reliable of the non-intrusive flow regime identification techniques tested. Several different display techniques complemented each other in creating a realistic view of the flow inside the channel. Void fraction measurements using ECT were compared to visualizations and energy balance calculations and proved to be fairly accurate and much less subjective than the high speed video analysis.

The discrete wavelet transform was used to generate a compact representation of the characteristic frequencies of two-phase refrigerant flow. The different flow regimes have recognizable frequency spectra that will hopefully provide for an automatic flow regime detection algorithm. Wavelet analysis has several benefits over Fourier analysis; the wavelet analysis can represent both time and frequency information. Also, it provides for a method of discretely binning the global energy spectrum of a signal whereas a similar Fourier analysis would require more user intervention.

The pressure drop observations from the current work fit into the widely variable correlations that were available in the literature. Comparing the current experimental data with Mishima and Hibiki[30] resulted in a MAE of 35%; however comparing the results between Yu et al.[31] and Lee and Lee[32] produced a MAE of 95%. This lack of uniformity shows the need for a method of producing a correlation to capture the physical behavior of two phase flow with the use of a more general correlation. Flow regime identification appears to be

very important in achieving this goal. Future work is expected to further the research identifying two phase flow regimes and investigating the possibility of a generalized correlation across channel size, shape, and fluid.

REFERENCES

[1]Thome, J. R., "State-of-the-Art Overview of Boiling and Two-Phase Flows in Microchannels," *Heat Transfer Engineering*, Vol. 27, No. 9, 2006, pp. 4-19.

[2]Qu, W., and Mudawar, I., "Measurement and Correlation of Critical Heat Flux in Two-Phase Micro-Channel Heat Sinks," *International Journal of Heat and Mass Transfer*, Vol. 47, No. 10-11, 2004, pp. 2045-2059.

[3]Zhang, H., Mudawar, I., and Hasan, M. M., "Photographic Study of High-Flux Subcooled Flow Boiling and Critical Heat Flux," *International Communications in Heat and Mass Transfer*, Vol. 34, No. 6, 2007, pp. 653-660.

[4]Tran, T. N., Chyu, M. C., Wambsganss, M. W., and France, D. M., "Two-Phase Pressure Drop of Refrigerants During Flow Boiling in Small Channels: an Experimental Investigation and Correlation Development," *International Journal of Multiphase Flow*, Vol. 26, No. 11, 2000, pp. 1739-1754.

[5]Lee, P. S., and Garimella, S. V., "Saturated Flow Boiling Heat Transfer and Pressure Drop in Silicon Microchannel Arrays," *International Journal of Heat and Mass Transfer*, Vol. 51, 2008, pp. 789-806.

[6]Brutin, D., Topin, F., and Tadrist, L., "Experimental Study of Unsteady Convective Boiling in Heated Minichannels," *International Journal of Heat and Mass Transfer*, Vol. 46, No. 16, 2003, pp. 2957-2965.

[7]Quiben, J. M., and Thome, J. R., "Flow Pattern Based Two-phase Frictional Pressure Drop Model for Horizontal Tubes, Part II: new Phenomenological Model," *International Journal of Heat and Fluid Flow*, Vol. 28, 2007, pp. 1060-1072.

[8]Kandlikar, S. G., "Heat Transfer Mechanisms During Flow Boiling in Microchannels," *Journal of Heat Transfer*, Vol. 126, No. 1, 2004, pp. 8-16.

[9]Dong, F., Liu, X., Deng, X., Xu, L., and Xu, L. A., "Identification of Two-phase Flow Regimes in Horizontal, Inclined and Vertical Pipes," *Measurement Science and Technology*, Vol. 12, 2001, pp. 1069-1075.

[10]Halow, J. S., and Nicoletti, P., "Observations of Fluidized Bed oalescence Using Capacitance Imaging," *Powder Technology*, Vol. 69, No. 3, 1992, pp. 255-277.

[11]Loser, T., Wajman, R., and Mewes, D., "Electrical Capacitance Tomography: Image Reconstruction Along Electrical Field Lines," *Measurement Science and Technology*, Vol. 12, No. 8, 2001, pp. 1083-1091.

[12]Peng, L., Jiang, P., Lu, G., and Xiao, D., "Window Function-Based Regularization for Electrical Capacitance Tomography Image Reconstruction," *Flow Measurement and Instrumentation*, Vol. 18, No. 5-6, 2007, pp. 277-284.

[13]Farge, M., "Wavelet Transorms and Their Applications to Turbulence," *Annual Review of Fluid Mechanics*, Vol. 24, 1992, pp. 395-457.

[14]Elperin, T., and Klochko, M., "Flow regime identification in a two-phase flow using wavelet transform," *Experiments in Fluids*, Vol. 32, 2002, pp. 674-682.

[15]Tan, D., Dong, F., and Megngmeng, W., "Identification of Gas/liquid Two-phase Flow Regime Through ERT-based Measurement and Feature Extraction," *Flow Measurement and Instrumentation*, Vol. 18, 2007, pp. 255-261.

[16]Daubechies, I., "Ten Lectures on Wavelets," *Society for Industrial and Applied mathematics*. 1992.

[17]Kumar, P., and Foufoula-Georgiou, E., "Wavelets in Geophysics," *Academic Press*, Vol. 4, 1994.

[18]Torrence, C., and Compo, G., "A Practical Guide to Wavelet Analysis," *Bulletin of the American Meteorological Society*, Vol. 79, No. 1, 1997, pp. 61-78.

[19]Tropea, C., Yarin, A. L., and Foss, J. F., *Springer Handbook of Experimental Fluid Mechanics*: Springer, 2007.

[20]Kreitzer, P. J., Byrd, L., and Willebrand, B. J., "Initial Investigation of Two Phase Flow Characterization of R134a in a Horizontal Channel using High Speed Video Analysis and Electrical Capacitance Tomography," *42nd AIAA Thermophysics Conference*. Hawaii, 2011.

[21]Huang, S. M., Xie, C. G., Thorn, R., Snowden, D., and Beck, M. S., "Design of Sensor Electronics for Electrical Capacitance Tomography," *Circuits, Devices and Systems, IEE Proceedings G*, Vol. 139, No. 1, 1992, pp. 83-88.

[22]Yang, W. Q., and Peng, L., "Image Reconstruction Algorithms for Electrical Capacitance Tomography," *Measurement Science and Technology*, Vol. 14, No. 1, 2003, pp. R1-R13.

[23]Huang, Z., Wang, B., and Li, H., "Application of Electrical Capacitance Tomography to the Void Fraction Measurement of Two-Phase Flow," *IEEE Transactions on Instrumentation and Measurement*, Vol. 52, No. 1, 2003, pp. 7-12.

[24]Warsito, W., and Fan, L. S., "Measurement of Real-Time Flow Structures in Gas–Liquid and Gas–Liquid–Solid Flow Systems using Electrical Capacitance Tomography (ECT)," *Chemical Engineering Science*, Vol. 56, No. 21-22, 2001, pp. 6455-6462.

[25]Yang, W. Q., Spink, D. M., York, T. A., and McCann, H., "An Image-Reconstruction Algorithm Based on Landweber's Iteration Method for Electrical-Capacitance Tomography," *Measurement Science and Technology*, Vol. 10, No. 11, 1999, pp. 1065-1069.

[26]Matlab, "Version 7.0," 7.10 ed., The MathWorks Inc., Natick, MA, 2010.

[27]Warrier, G. R., Dhir, V. K., and Momoda, L. A., "Heat Transfer and Pressure Drop in Narrow Rectangular Channels," *Experimental Thermal and Fluid Science*, Vol. 26, No. 1, 2002, pp. 53-64.

[28]Wilkens, R. J., and Thomas, D. K., "A Simple Technique for Determining Slug Frequency Using Differential Pressure," *Journal of Energy Resources Technology*, Vol. 130, No. 1, 2008, pp. 014501-6.

[29]Carey, V. P., *Liquid-Vapor Phase-Change Phenomena*. New York, NY: Taylor & Francis Group, LLC., 2007

[30]Mishima, K., and Hibiki, T., "Some Characteristics of Air-water Two-phase Flow in Small Diameter Vertical Tubes," *International Journal of Multiphase Flow*, Vol. 22, No. 4, 1996, pp. 703-712.

[31]Yu, W., France, D. M., Wambsganss, M. W., and Hull, J. R., "Two-phase Pressure Drop, Boiling Heat Transfer, and Critical Heat Flux to Water in a Small-diameter horizontal Tube," *International Journal of Multiphase Flow*, Vol. 28, 2002, pp. 927-941.

[32]Lee, H. J., and Lee, S. Y., "Heat Transfer Correlation for Boiling Flows in Small Rectangular Horizontal Channels with Low Aspect Ratios," *International Journal of Multiphase Flow*, Vol. 27, 2001, pp. 2043-2062.

[33]Lockhart, R. C., and Martinelli, R. C., "Proposed Correlation of Data for Isothermal Two-phase, Two-component Fow in Pipes," *Chemical Engineering Progress*, Vol. 45, 1949, pp. 39-48.

[34]Qu, W., and Mudawar, I., "Measurement and Prediction of Pressure Drop in Two-phase Micro-channel Heat Sinks," *International Journal of Heat and Mass Transfer*, Vol. 46, 2003, pp. 2737-2753.